

BRINE PERMEABILITY PREDICTIONS FOR SAND PACKS AND SANDSTONES USING NAVIER-STOKES EQUATIONS AND THREE-DIMENSIONAL MICROTOMOGRAPHY IMAGES OF PORE SPACES

Shakil AHMED^{1*} and Stefan IGLAUER²

¹ CSIRO Earth Science and Resources Engineering, Kensington, WA 6151, AUSTRALIA

² Department of Petroleum Engineering, Faculty of Science and Engineering, Curtin University of Technology,
Kensington, WA 6151, AUSTRALIA

*Corresponding author, E-mail address: Shakil.Ahmed@csiro.au

ABSTRACT

A sand pack and a sandstone were imaged with micro-computed tomography at nominal voxel sizes of approximately $(6\mu\text{m})^3$. From these images the pore morphologies of the porous media were obtained by segmentation. The segmented images were then used to generate surface and volume meshes of pore spaces for flow analysis. Three-dimensional, steady state, isothermal, incompressible single phase fluid flow fields were obtained by solving the continuity and Navier-Stokes equations. An inlet boundary condition was set by specifying the brine injection velocity while a pressure boundary condition was prescribed at the outlet, which resulted in laminar flow, and which is representative of flow in aquifers or oil reservoirs. From the pressure and velocity vector fields we computed the total pressure drop across the sample and the area-averaged velocity at the inlet with which we then determined brine permeability for each porous medium. The predicted permeabilities were consistent with experimental core-flood data; the presented approach is therefore a rapid and cost-effective method to determine single-phase permeabilities of incompressible fluids in porous media. Only small dry rock fragments are required for the described analysis.

NOMENCLATURE

k	permeability of the porous rock (m^2)
p	pressure
q	volumetric flow rate (m^3/sec)
S	source or sink term
\mathbf{u}	velocity
u	area average inlet velocity (m/sec)
$\frac{dp}{dl}$	pressure gradient in the direction of the flow, Pa/m
ρ	density
μ	dynamic viscosity of the fluid (Pa.s)

INTRODUCTION

Permeability is the most important petrophysical parameter apart from porosity and it determines the economics and technical feasibility of hydrocarbon recovery operations and carbon geo-sequestration projects. Typically, permeability is measured in the laboratory by injecting air through a cylindrical core plug at a constant flow rate and simultaneously measuring the pressure drop

over the core length. Air is used in this standard measurement because the measurement can then easily and rapidly be performed; however, because air molecules have a mean free path larger than the pore sizes of the rock, which results in slippage of the gas along the solid pore surface, an adjustment ("Klinkenberg correction") needs to be applied in order to estimate brine permeabilities (which are far more relevant in a Petroleum Engineering context, Tiab and Donaldson, 2004). In addition, care needs to be taken to avoid turbulent flow in the air stream, so a sufficiently low flow rate needs to be chosen to stay in the laminar flow regime; furthermore air compressibility is high, while brine is almost incompressible. It is therefore clear that a brine permeability measurement provides superior data for reservoir simulations, but a direct brine measurement is more cumbersome and time-consuming and therefore more expensive. A rapid and cost-effective alternative to experimental permeability measurements is the computation of brine permeabilities. Such a calculation can be approached in different ways, e.g. using pore-network models (compare for instance Dong and Blunt, 2009). Such pore-networks can be generated by various methods, but they all have in common that they strongly simplify the complex pore morphology, which again limits their predictive power. Another ansatz is the Lattice Boltzmann method or Computational Fluid Dynamics (CFD). We focus here on CFD as it is the most accurate computation, as the full Navier-Stokes equations are solved (numerically). Our approach is as follows: we extracted the pore morphology of the porous media from 3D micro-computed tomography (μ -CT) images, which captured the structure of the pore space accurately with resolutions in the micrometer range (Iglauer et al. 2010). We convert these images into mathematical meshes and use CFD to predict brine permeability. Our approach is based on earlier similar work, where permeabilities were calculated by solving the Stokes or Navier-Stokes equations and tomographic images as an input parameter (e.g. Zaretskiy et al. 2010, Mostaghimi et al. 2010, Ovaysi and Piri 2011).

The main limitation of the computational approaches is the limited size of the volume element studied (millimetre scale). In the following we describe in detail how the images were acquired and mathematical meshes were extracted on which the CFD calculations were performed. We then compare our simulation results with experimental data in the results section and find good consistency.

DESCRIPTION OF THE POROUS MEDIA

Two samples, an Ottawa F-42 sand pack and Doddington sandstone were selected for this investigation, figure 1(a) and 1(b). Details about the petrophysical and petrochemical properties of the samples are described elsewhere (Gittins et al. 2010, Iglauer et al. 2010).

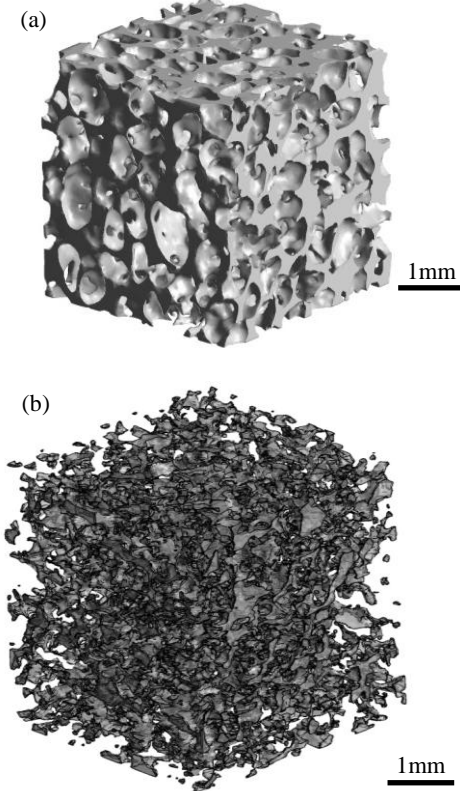


Figure 1: (a) F-42 sand pack showing the pore spaces only, the holes in the sample represent the grains and (b) Doddington sandstone pore spaces after separating from grain.

μ -CT images of both samples were acquired as outlined in detail below. Image dimensions for both images were 300x300x300 voxels (i.e. approximately 5.83 mm³ for the Doddington sandstone and 10.29 mm³ for the F-42 sand pack). Pore spaces were separated from grains after segmentation with image processing software (Avizo); from the binarized images volume meshes were generated for the CFD computations. The procedures in terms of acquiring the μ -CT images, segmentation and volume mesh generation are explained in more detail below.

Acquiring μ -CT images

For the acquisition of the Doddington sandstone μ -CT image, a small cylindrical core plug with a diameter of 5mm and a length of 10mm was drilled. A subvolume of this plug was then scanned with a Phoenix v/tome/x microtomograph at a nominal resolution of 5.999 μ m. To obtain an image of the Ottawa F-42 sand pack, a hollow plastic tube with an inner diameter of 5mm, and a thin wall was sealed at one end with a plastic plug, and the tube was carefully packed with sand by first pouring the sand continuously into the tube and then tapping the tube and adding a small amount of additional sand. The tube was then sealed at its top and a subvolume of the sand pack was imaged at a nominal resolution of 7.250 μ m.

Processing μ -CT images for numerical modelling

A μ -CT image is a 3D greyscale image, each greyscale tone corresponds to the x-ray mass absorption coefficient of the specific voxel (volume element). For any quantitative analysis, the greyscale values need to be assigned to different phases, in our case the rock phase or the air phase. Indeed the accuracy of the absolute permeability computations depends strongly on this segmentation as discussed further below. We analysed 3D sample by stacking 2D images (figure 2(a)).

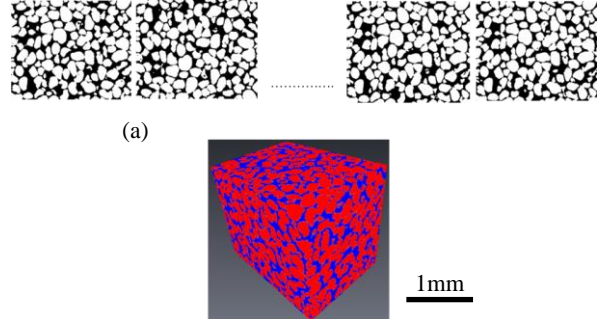


Figure 2(a): 2D μ -CT image slices are stacked together to generate the 3D F-42 sand pack sample and subsequently the F-42 volume mesh.

The pore spaces (air phase) were used to generate a triangular surface mesh. The quality and ability of the triangular surface mesh to generate the tetrahedral volume mesh was checked with orientation, intersection and tetra quality. The surface mesh was then imported into a powerful mesh generating software, ICEMCFD, to generate the volume mesh. Initially the volume mesh of the whole pore spaces was generated. For the flow analysis, to save computational expense, all disconnected pore spaces were truncated out of the mesh; such disconnected void space does not contribute to permeability. For example, Figure 1(b) shows all the pore spaces for Doddington sandstone while Figure 2(b) shows only the connected pore spaces which were considered for numerical modelling.

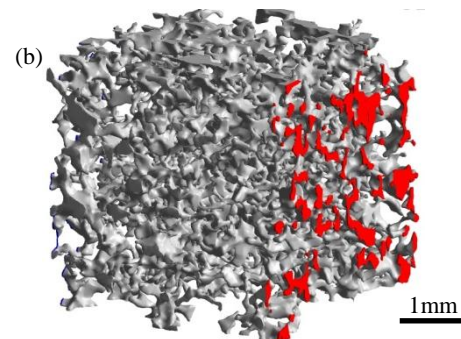


Figure 2(b): connected pore spaces of Doddington sandstone used in numerical modelling. Red area represents the flow inlet.

NUMERICAL MODELLING

In order to predict brine permeability, we solved the continuity (equation 1) and Navier-Stokes (equation 3) equations.

$$\frac{\partial \rho}{\partial t} + \nabla \cdot (\rho \mathbf{u}) = 0 \quad (1)$$

$$\frac{\partial \rho \mathbf{u}}{\partial t} + \nabla \cdot (\rho \mathbf{u} \mathbf{u}) = -\nabla p + \nabla \cdot \mu \nabla \mathbf{u} + \mathbf{S} \quad (2)$$

We assumed steady state and no chemical reaction, so the unsteady state term $\frac{\partial \rho}{\partial t}$ and \mathbf{S} were set to zero, ρ is the fluid density, \mathbf{u} is the velocity vector, and t is time.

The computations were performed using a commercially available CFD package (ANSYS-CFX), which has a coupled solver (simultaneously solves u , v , and w momentum of the Navier-Stokes equation, different from SIMPLE algorithm) and uses an unstructured mesh based on element based finite volume (FV) method (Ferziger and Peric, 1997). FV uses the integral form of the conservation equations as its starting point. The solution domain is subdivided into a finite number of contiguous control volumes (CVs), and the conservation equations are applied to each CV. At the centroid of each CV lies a computational node at which the variable values are to be calculated. FV can accommodate any type of grid, so it is suitable for complex geometries. The grid defines only the control volume boundaries and need not be related to a coordinate system.

A uniform brine injection velocity inlet boundary condition was specified, and a pressure boundary condition was prescribed at the outlet (opposite side of inlet), this reference pressure was set to 0. All the other faces were assumed to be impermeable, which was obtained by applying no-slip wall boundary conditions. These boundary conditions were chosen in a way that the experimental measurement procedure (Pentland et al. 2008, Gittins et al. 2010) was closely replicated. Table 1 summarizes the boundary conditions and associated values and other input parameters.

parameter	symbol	value
brine injection velocity into F-42 sand pack	U_i	10^{-3} m/s
brine injection velocity into Doddington sandstone	U_i	5×10^{-4} m/s
no-slip boundary condition at four walls	U_i	0
outlet pressure	p	0
brine density	ρ	1040 kg/m^3
brine viscosity	μ	$\sim 10^{-3} \text{ Pa.s}^{#1}$

Table 1: Summary of applied boundary conditions and input parameters. #1 Lide 2006.

The pressure at the inlet is therefore equal to the pressure difference between inlet and outlet, i.e. the pressure drop across the sample. Figure 3(a) shows the boundary conditions for the F-42 sand pack. Approximately 2.0 million tetrahedral elements were used to generate the meshes. A sample mesh for the F-42 sand pack is shown in Figure 3(b). The convergence criterion for all variables was set to 10^{-5} .

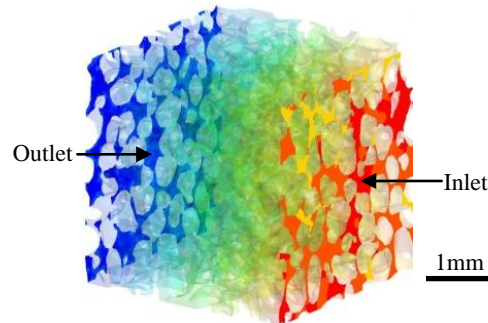
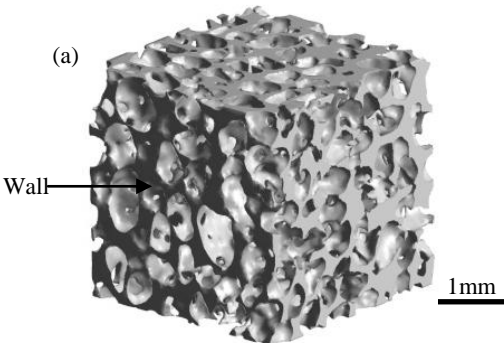


Figure 3(a): boundary conditions for F-42 sand pack. Red indicates brine inlet and blue indicates pressure outlet

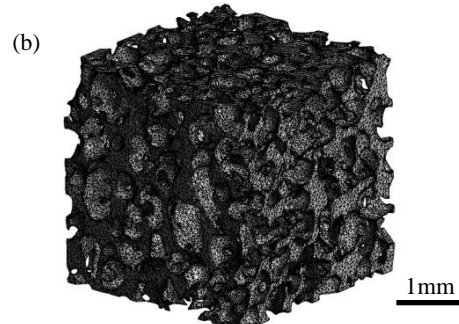


Figure 3(b): volume mesh of F-42 sand pack used for absolute permeability calculation.

Grid Independence Test

The grid independence test was performed on the Doddington sandstone mesh and the solutions were grid independent when the total number of elements was around 2 million. Starting with a coarse grid the number of elements was increased gradually and each time pressure drop across the sample was plotted. When the pressure drop for two successive grid refinements was nearly unchanged (1% variation) the solutions were considered grid independent.

RESULTS AND DISCUSSION

We calculated the pressure field and the velocity vector fields over all grid elements with CFD. From this information we computed the pressure gradient across the sample length (dp/dl), and used Darcy's law (equation 3) to calculate the absolute permeability k .

$$u = \frac{q}{A} = -\frac{k}{\mu} \frac{dp}{dl} \quad (3)$$

Where u is the area average inlet velocity, A is the cross-sectional area of the sample, here area at the inlet, μ is the brine viscosity, and q is the volumetric flow rate.

Results for F-42 sand pack

Figure 4(a) shows the pressure distribution at the inlet. The maximum predicted pressure was 45 Pa, and the predicted area-averaged pressure was 37 Pa. Inserting this area average pressure into Darcy's equation, a brine permeability of 43 Darcy was predicted, which is in excellent agreement with the experiments (42.0 ± 4.0 Darcy, Gittins et al. 2010, Talabi et al. 2009). Figure 4(b) shows the pressure distribution at the pore wall.

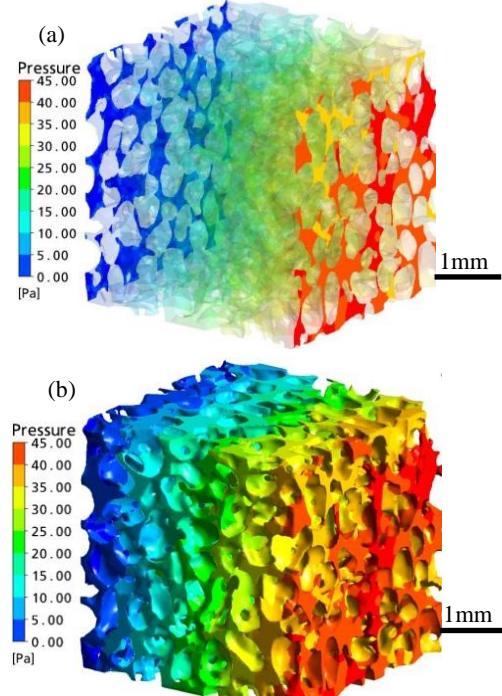


Figure 4(a-b): pressure distribution (a) at inlet and (b) at the pore wall.

The pressure contour at the mid plane (parallel to the flow direction) is shown in Figure 5(a-b). Flow direction is from right to left. The pressure gradually dropped from 45 Pa to 0. Velocity contours and vectors in the same plane are shown in Figure 6(a-b) from which the area of maximum velocity can be identified.

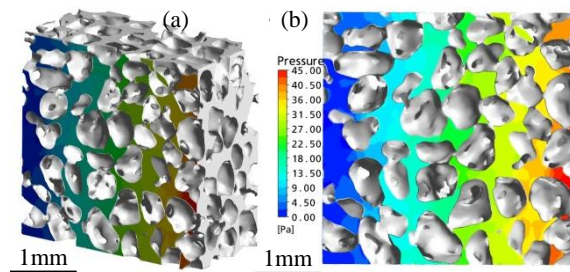


Figure 5(a-b): (a) cross sectional plane parallel to the flow and (b) pressure contour in that plane for the F-42 sand pack.

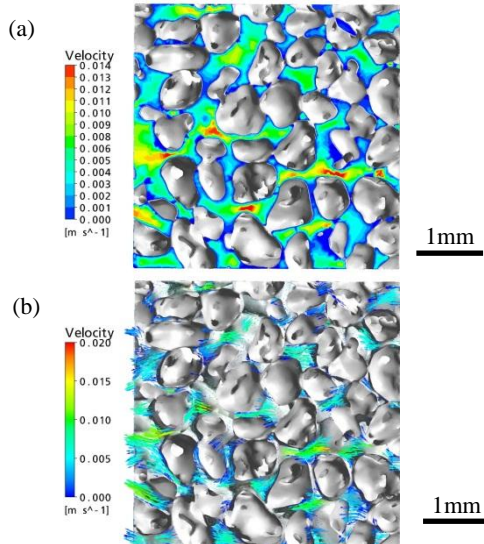


Figure 6(a-b): (a) velocity contour and (b) velocity vector at the mid plane along the flow for the F-42 sand pack. The flow is from right to left.

Results for Doddington sandstone

The pressure distribution on the pore walls for Doddington sandstone is displayed in Figure 7. The maximum predicted pressure at the inlet was 200 Pa, and the area-averaged pressure at the inlet used for the absolute permeability calculation was 176 Pa. The predicted absolute permeability for the Doddington sample was 4.0 Darcy, while the measured permeability was in the range of 1.5-2.0 Darcy (Iglauer et al. 2011a, b)

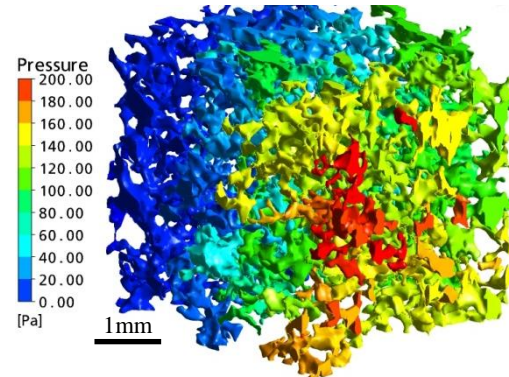


Figure 7: pressure distribution at the pore wall for Doddington sandstone.

Differences between experimental and computed permeability -and this is one of the main limitations of our approach- may be caused by sample heterogeneity and the fact that only a small sub-volume is investigated in the computation, while typically the experimental data is measured on much larger samples; this effect is not very strong in a fairly homogeneous sand pack, but we expect this effect to be very significant if the porous medium is highly heterogeneous, as for example in some carbonate rocks. However, in case of the studied Doddington sandstone, which is fairly homogeneous, we believe that the fairly high deviation between predicted and measured permeability ($\approx 100\%$) is due to image segmentation. Indeed, from our earlier μ -CT studies (Iglauer et al. 2010, 2011a, c, 2012a, b) we learned that there is a degree of uncertainty associated with selecting a threshold (note that

simply applying some standardized mathematical algorithms is likely to result in poor quality segmentation, and for a good segmentation a sequence of algorithms needs to be applied in an iterative process). And although the segmentation effect is not significant in terms of porosity (if sufficient care is taken), it can have a strong effect on permeability calculations, because permeability is very sensitive to pore throat radius r (recall that the Hagen-Poiseuille equation predicts that $dP/dr \propto r^4$). This again means that by selecting different thresholds, which vary by only a few voxel layers, significant changes in the permeability predictions may result. In our future analysis we will tune our “geometrical model” – i.e. the mathematical mesh of the pore space so that it accurately predicts the experimental permeability before embarking on more complex calculations.

Figure 8(a) shows the pressure distribution at the mid plane parallel to the flow. The flow is from right to left. Figure 8(b) shows the velocity contour in the same plane. The location of the maximum velocity was identified and the value was 5×10^{-3} m/sec. Table 2 summarizes the measured and predicted petrophysical properties.

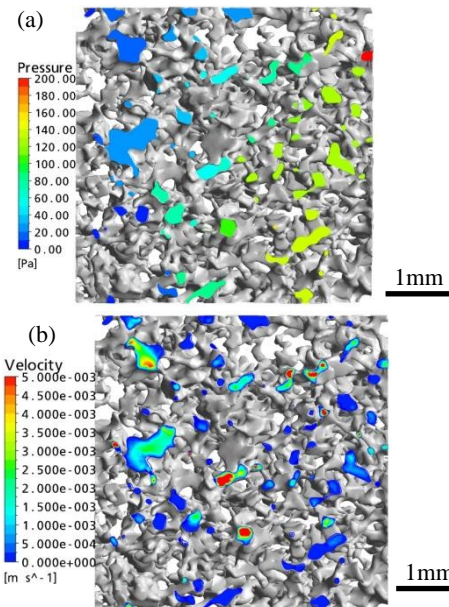


Figure 8(a-b): (a) pressure contour and (b) velocity contour at the mid plane parallel to the flow for Doddington sandstone. The flow is from right to left.

parameter	sand pack Ottawa F-42	sandstone Doddington
porosity (measured)	$35.0 \pm 0.2\%^{#1}$	$20.5\%^{#2}$
porosity (from μ -CT image)	34.8%	20.7%
brine permeability (measured)	$42.0 \pm 2.1 D^{#1}$	$1.6 D^{#2}$
brine permeability (computed)	43D	4D

Table 2: Measured and computed petrophysical properties. #1 Gittins et al. 2010; #2 Iglauser et al. 2011b

CONCLUSION

We investigated the prediction of brine permeability of a sand pack and a sandstone using full Navier-Stokes equations and three dimensional μ -CT images of pore spaces. This is a relatively new approach for the analysis of transport phenomena in porous media at the pore-scale. Alternative available methods use either an approximation of the real geometry (network models) or solve a simplified mathematical model (Lattice-Boltzmann method). Our approach is therefore more fundamental with a higher predictive power. We demonstrated that we can predict brine permeabilities of sand packs and sandstones; the predicted value for the investigated sand pack was consistent with experimental values, while the sandstone permeability was over predicted by a factor of approximately 2. We think that this discrepancy is mainly due to μ -CT image segmentation, but also due to sample heterogeneity (the experimental and computational volumes are different). Nevertheless the consistency is good considering that the experiment also has an error; and in the future with μ -CT images acquired at higher resolutions (submicron resolution is achievable nowadays with state-of-the-art equipment) the thresholding error will be mitigated.

REFERENCES

- DONG, H., BLUNT, M.J.(2009), “Pore-network extraction from micro-computerized-tomography images”, *Physical Review E*, 80, 036307.
- FERZIGER, J.H., and PERIC, M. (1997), “Computational Methods for Fluid Dynamics”, *Springer-Verlag-Berlin Heidelberg New York*.
- GITTINS, P., IGLAUER, S., PENTLAND, C.H., AL-MANSOORI, S.K., AL-SAYARI, S., BIJELJIC, B., BLUNT, M.J.(2010), “Non-wetting phase residual saturation in sand packs”, *Journal of Porous Media*, 13, 7, 591-599.
- IGLAUER, S., FAVRETTO, S., SPINELLI, G., SCHENA, G., BLUNT, M.J. (2010), “X-ray tomography measurements of power-law cluster size distributions in sandstones”, *Physical Review E*, 82, 5, 056315.
- IGLAUER, S., PALUSZNY, A., PENTLAND, C.H., BLUNT, M.J. (2011a), “Residual CO₂ imaged with x-ray micro-tomography”, *Geophysical Research Letters*, 38, L21403.
- IGLAUER, S., WÜLLING, W., PENTLAND, C.H., AL-MANSOORI, S.K., BLUNT, M.J.(2011b), “Capillary trapping capacities of consolidated rocks and sands”, *SPE Journal*, 16, 4, 778-783.
- IGLAUER, S., WANG, S., RASOULI, V. (2011c), “X-ray micro-tomography measurements of fractured tight sandstone”, SPE 145960, SPE Asia Pacific Oil and Gas Conference and Exhibition, Jakarta, Indonesia, 20-22nd September.
- IGLAUER, S., FERNØ, M., SHEARING, P., BLUNT, M.J. (2012a), “Comparison of residual oil cluster size distribution, morphology and saturation in oil-wet and water-wet sandstone”, *Journal of Colloid and Interface Science*, 375, 1, 187-192.
- IGLAUER, S., PALUSZNY, A., BLUNT, M.J. (2012b), “Simultaneous oil recovery and residual gas storage: a pore-level analysis using in-situ micro-tomography”, *Fuel*, in press.

LIDE, D.R. ed. (2006), "CRC Handbook of Chemistry and Physics", 87th edition. Boca Raton, Florida: CRC Press.

MOSTAGHIMI, P., BIJELJIC, B., BLUNT, M.J. (2010), "Simulation of flow and dispersion on pore-space images", SPE 135261, SPE Annual Technical Conference and Exhibition, Florence, Italy, 19-22nd September.

OVAYSI, S., PIRI, M. (2011), "Pore-scale modelling of dispersion in disordered porous media", *Journal of Contaminant Hydrology*, 124, 68-81.

PENTLAND, C.H., AL-MANSOORI, S.K., IGLAUER, S., BIJELJIC, B., BLUNT, M.J.(2008), "Measurement of non-wetting phase trapping in sand packs", SPE 115697, SPE Annual Technical Conference and Exhibition, Denver, Colorado, USA, 21-24th September.

TALABI, O., AL-SAYARI, S., IGLAUER, S., BLUNT, M.J. (2009), "Pore-scale simulation of NMR response", *Journal of Petroleum Science and Engineering*, 67, 168-178.

TIAB, D., DONALDSON, E.C., (2004), "Petrophysics", *Amsterdam: Elsevier*.

ZARETSKIY, Y., GEIGER, S., SORBIE, K., FÖRSTER, M. (2010), "Efficient flow and transport simulations in reconstructed 3D pore geometries", *Advances in Water Resources*, 33, 1508-1516.

ACKNOWLEDGEMENT

The authors wish to acknowledge financial assistance provided through Australian National Low Emissions Coal Research and Development (ANLEC R&D). ANLEC R&D is supported by Australian Coal Association Low Emissions Technology Limited and the Australian Government through the Clean Energy Initiative (ANLEC project 3-0911-0155).